Comprehensive Exam

Criston Hyett

June 23, 2023

1 Introduction

This manuscript is an example-driven survey of broadly termed "data-enhanced dynamical systems modeling" (DataDyn). Underneath the umbrella of DataDyn, I allow any enriching of theoretical dynamical systems modeling with data. I will focus on the not exhaustive list of:

- parameterizing ODE/PDE/SDEs at a variety of levels
  - single parameter searches
  - fitting neural networks to define dynamics
  - parameterized boundary condition determination
- creating reduced-order models (ROM) via applying projection methods to data
  - linear (PCA/POD) methods
  - nonlinear autoencoder/decoder
- using differentiable programming (DP) and automatic differentiation to allow for automatic sensitivity calculation of DE solutions w.r.t. parameterizations
- applying specifically structured neural networks to improve interpretability and generalizability
- learning discretizations for PDEs

2 Lagrangian Reduced-Order Models for Homogenous Isotropic Turbulence

The dynamics of the velocity gradient tensor provide a privileged view into important characteristics of turbulence, some of which include: local fluid deformation, strain, energy cascade, and intermittency. Recent work using Tensor Basis Neural Network for the evolution of the velocity gradient tensor has performed very well. In this work we closely examine the individual contributions from the components of this physics-informed machine learning framework in search of interpretability. We find that not all components contribute to the prediction, and thus an even simpler description is possible. We conclude by postulating physical justification of this further-reduced description.

2.1 Introduction

Turbulence being a widespread phenomenon, an enormous body of work is dedicated to modeling and simulating it. Resulting from this plethora of simulation efforts are enormous datasets. Recently, with the advances of machine learning - particularly physics-informed machine learning - data-driven models regularly out-perform phenomenological models, suggesting that these large datasets contain exploitable patterns that we don't yet recognize.

At the same time, the promise of physics-informed machine learning is that via imposing structure on the infuriatingly flexible neural network, one might simultaneously improve generalizability (i.e., learn not just data patterns, but physical laws), and have those learned models be interpretable.

Our work focuses on the Lagrangian perspective of turbulence, centering ourselves on the statistical evolution of the velocity gradient tensor (VGT). Recent work [**?**] constructed the so called "Tensor Basis Neural Network" (TBNN), and trained it to learn the pressure Hessian contribution to the evolution of the VGT.

In this work we will present the TBNN formulation, reiterate the results of Tian et.al, and show that by examining the trained model, one can tease out physically relevant patterns, toward the hope of learning new physics.

2.2 Tensor Basis Neural Network

We begin with Navier-Stokes for an incompressible fluid:

$$\frac{\partial u_i}{\partial t} + u_k \frac{\partial u_i}{\partial x_k} = -\frac{\partial P}{\partial x_i} + \nu \frac{\partial^2 u_i}{\partial x_k \partial x_k} \tag{1}$$

then, as the velocity gradient tensor is defined as $A_{ij} = \frac{\partial u_i}{\partial x_j}$, we apply spatial derivatives, and use the definition of material derivative ($\frac{dA_{ij}}{dt} = \frac{\partial A_{ij}}{\partial t} + u_k \frac{\partial A_{ij}}{\partial x_k}$) to get:

$$\frac{dA_{ij}}{dt} = \frac{\partial A_{ij}}{\partial t} + u_k \frac{\partial A_{ij}}{\partial x_k} = -A_{ik}A_{kj} - \frac{\partial^2 P}{\partial x_i \partial x_j} + \nu \frac{\partial^2 A_{ij}}{\partial x_k \partial x_k} \tag{2}$$

Additionally, from incompressibility, we have

$$\frac{\partial^2 P}{\partial x_k \partial x_k} = -A_{ij}A_{ji} \tag{3}$$

This allows us to define the nonlocal deviatoric part of the pressure hessian

$$H_{ij} = -\left(\frac{\partial^2 P}{\partial x_i \partial x_j} - \frac{1}{3} \frac{\partial P}{\partial x_k \partial x_k} \delta_{ij} \right) \tag{4}$$

We can write the formal (nonlocal) solution for the deviatoric pressure hessian as[**?**]

$$H_{ij}(\mathbf{x}) = \iiint \frac{\delta_{ij} - \hat{r_i}\hat{r_j}}{2\pi r^3} Q(\mathbf{x} + \mathbf{r}) d\mathbf{r} \tag{5}$$

Following Lawson & Dawson[**?**], an expansion of the integral is proposed, first as a Taylor series expansion in $Q(x+r)$

$$\hat{H} = \sum_{m,n=0}^{\infty} \alpha_{mn} S^m W^n \tag{6}$$

where

$$S = \frac{1}{2}(A + A^T) \qquad W = \frac{1}{2}(A - A^T) \tag{7}$$

Finally we can reduce from an infinite sum using Cayley-Hamilton, and expand via the tensor basis[**?**]

$$\hat{H} = \sum_{n=1}^{10} g^{(n)}(\lambda_1, \ldots, \lambda_5) T^{(n)} \tag{8}$$

with $g^{(n)}$ scalar functions of the invariants

$\lambda_1 = \mathrm{tr}(S^2) \quad \lambda_2 = \mathrm{tr}(W^2) \quad \lambda_3 = \mathrm{tr}(S^3) \quad \lambda_4 = \mathrm{tr}(W^2 S) \quad \lambda_5 = \mathrm{tr}(W$

and the tensor basis given by:

$T^{(1)} = S$ $\qquad$ $T^{(2)} = SW - WS$

$T^{(3)} = S^2 - \frac{1}{3} I \cdot \mathrm{tr}(S^2)$ $\qquad$ $T^{(4)} = W^2 - \frac{1}{3} I \cdot \mathrm{tr}(W^2)$

$T^{(5)} = WS^2 - S^2 W$ $\qquad$ $T^{(6)} = W^2 S + SW^2 - \frac{2}{3} I$

$T^{(7)} = WSW^2 - W^2 SW$ $\qquad$ $T^{(8)} = SWS^2 - S^2 WS$

$T^{(9)} = W^2 S^2 + S^2 W^2 - \frac{2}{3} I \cdot \mathrm{tr}(S^2 W^2)$ $\qquad$ $T^{(10)} = WS^2 W^2 - W^2 S^2 V$

We use the natural timescale $\tau = \langle \| S^2 \|_2 \rangle^{-1}$ to normalize our VGT, and thus all of the $\lambda_i, T^{(j)}$. This formulation reduces the challenge to finding the functions of known scalars, i.e., learning the $g^{(n)}$'s.

$$\hat{H} = \sum_{i=1}^{10} g_\theta^{(i)}(\lambda_1, \ldots, \lambda_5) \cdot \hat{T}^{(i)}(\hat{A}) \tag{9}$$

$\lambda_1 = \mathrm{tr}(\hat{S}^2) \quad \lambda_2 = \mathrm{tr}(\hat{W}^2) \quad \lambda_3 = \mathrm{tr}(\hat{S}^3) \quad \lambda_4 = \mathrm{tr}(\hat{W}^2 \hat{S}) \quad \lambda_5 = \mathrm{tr}(\hat{W}$

$$L(\theta) = \frac{1}{N} \sum^{N} \left\| \hat{H}_{\text{truth}} - \sum_{i=1}^{10} g_\theta^{(i)}(\lambda_1, \ldots, \lambda_5) T^{(i)} \right\|_2^2 \tag{10}$$

2.3 Results

Previous phenomenological models have used truncated tensor basis expansions, with constant coefficients fit from averaging over data, to model the pressure Hessian contribution. From investigating the trained parameterization of the full expansion, we can investigate these choices.

To examine the learned model, we first investigate the sensitivity of the scalar functions $g_\theta^{(i)}$ to the variability of the invariants λ_j. This sensitivity will inform the learned "importance" of the λ_i to each $g_\theta^{(i)}$. In particular, we see in figure 1 that $g^{(9)}$ has large sensitivity to changes in λ_1, while nearly no sensitivity to λ_4 or λ_5. In fact, all of the scalar functions seem to depend only on λ_1, λ_2. We can test this hypothesis by training a new TBNN using only the first two invariants.

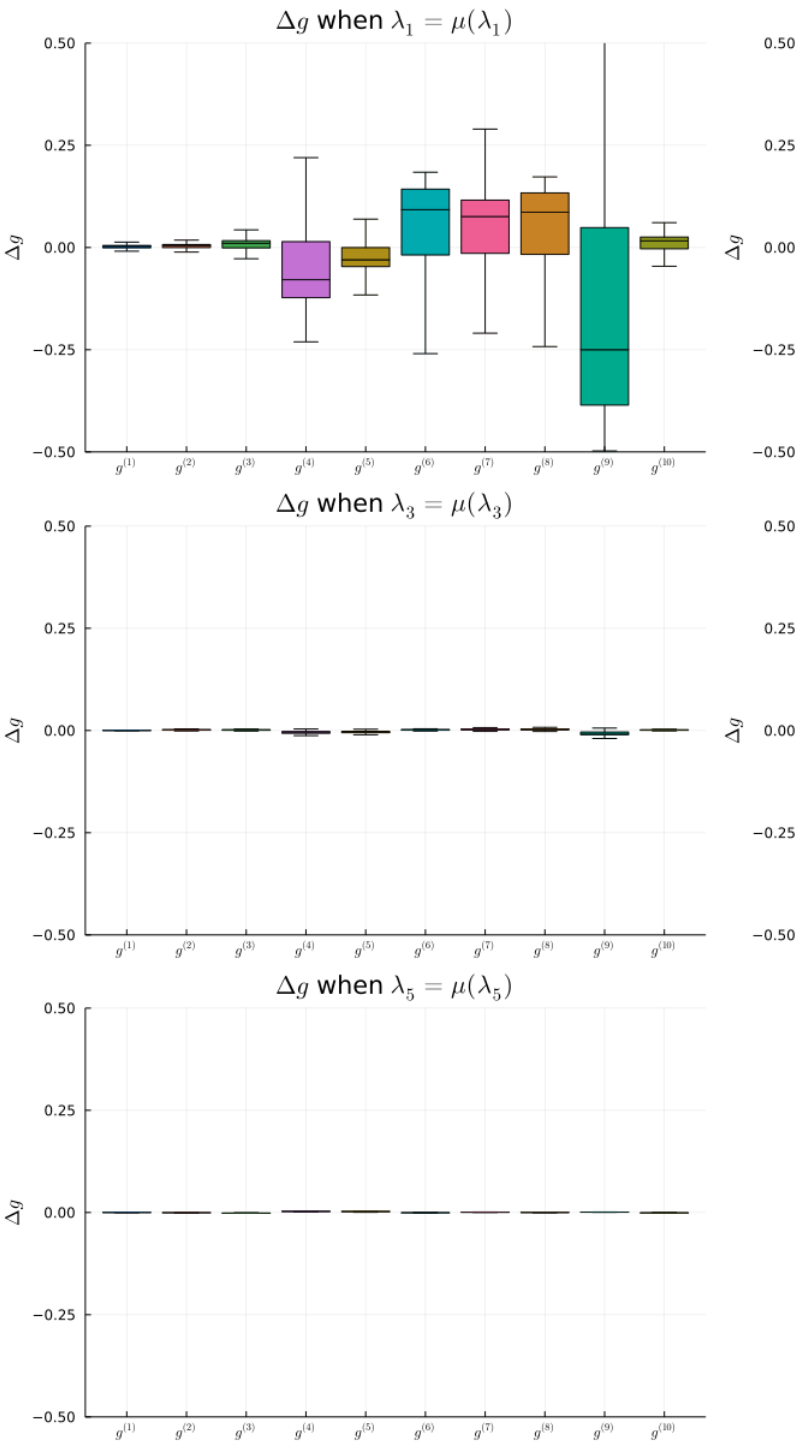

Figure 1:

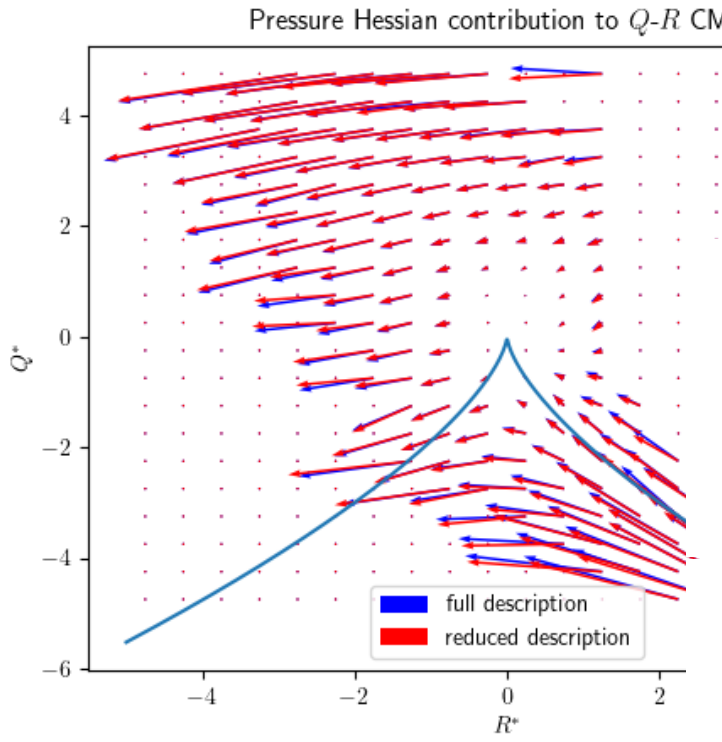

Figure 2:

A comparison between the two predictions of the pressure Hessian contribution is shown in figure[2].

We see that the change in prediction is very small - and within retraining error. Further, we can plot the g's to investigate the functional dependence on the λ_1, λ_2, using k-nearest neighbors algorithm to interpolate between datapoints.

2.4 Conclusion

3 Delivery of Natural Gas Under Uncertainty

We build and experiment with a realistic but reduced natural gas model of Israel. The system is unusual because (a) it is controlled from a limited number of points which are at, or close to, the gas extraction sites offshore of Israel's Mediterranean coast; (b) control specifies average flux at inlet, not pressure; (c) there are no inland compressors to regulate pressure; (d) power system is the main consumer of gas (70% of Israel's power is generated at gas-fired power plants distributed across the country). Nature of the system suggests that a special attention should be given to understanding dynamics driven by fast transients in gas consumption meeting intra-day variations in the electricity demand, and accounting for increasing role of uncertain renewable generation (mainly solar). Based on all of the above we pose and resolve a sequence of dynamic and control challenges, such as: How to time ramping up- and down- injection of gas to guarantee a healthy intra-day line-pack which meets both pressure constraints and gas-extraction patterns? We report simulation

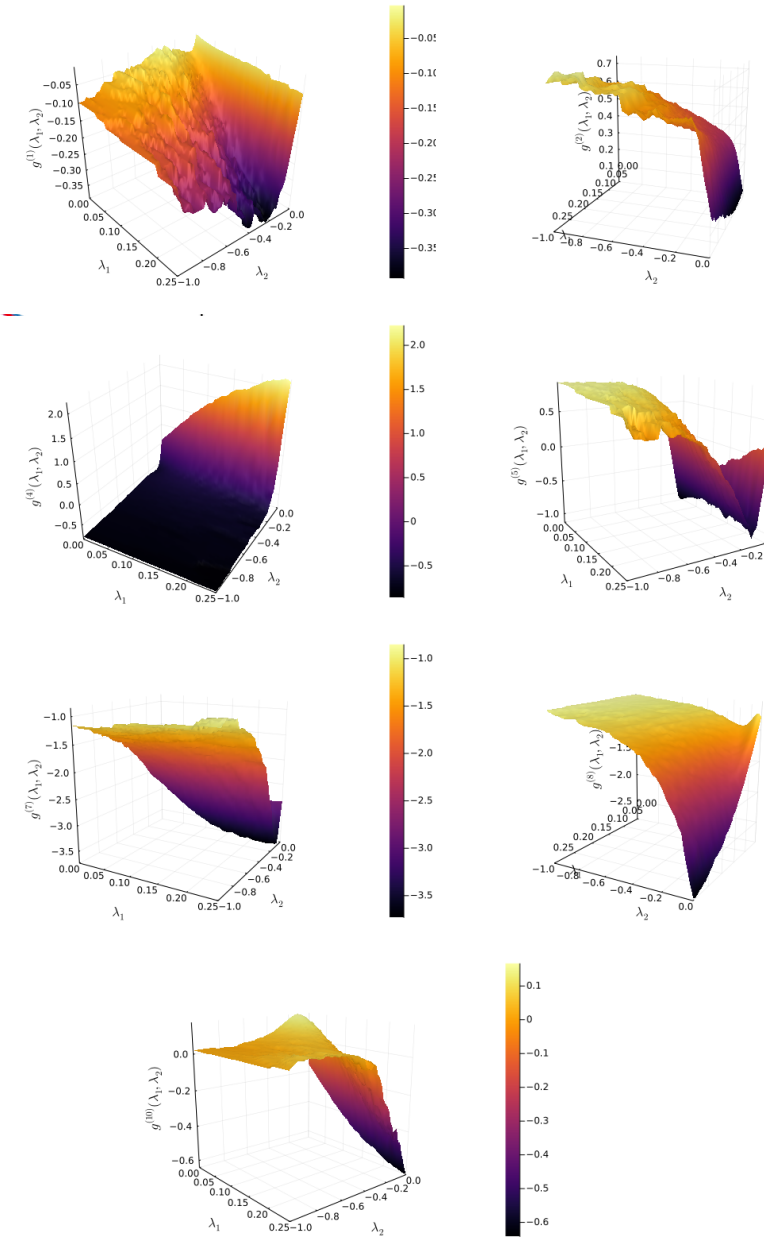

Figure 3:

results and utilize monotonicity properties of the natural gas flows which render robustness of our conclusions to the uncertainties of the edge withdrawals of gas.

4 Introduction

This is the first manuscript of the joint NOGA (Power System Operator of Israel) and UArizona team. We aim in this manuscript

- To explain specifics of the Natural Gas system of Israel, describe its minimal model and formulate main operational challenges related to uncertainty in production and consumption, also amplified by limited availability of resources. [Section 5]
- To describe basic modeling tools which allow us to study the system, including description of equations and of the software utilized. [Section 6]
- To formulate operational scenarios, reflecting the aforementioned uncertainty, and present analysis and control solutions. [Section 7]
- To sketch further plans to extend the demonstrated methodologies towards (a) joint, and thus more realistic, modeling and control of natural gas and power systems of Israel; but also (b) formulating further practical and academic challenges towards exporting the developed methodology to other energy systems of the size comparable to the one of Israel. [Section 9.]

5 Motivation, Data & Sources

Following the signing of the global agreement at the Paris Climate Conference in 2015, Israel set long-term goals to reduce greenhouse gas emissions in an effort to take part in the global action against climate change. Since the discovery of substantial offshore gas fields off the coast of Israel, Natural Gas (NG) has become the main fuel for electricity production in the country. In order to reduce Israel's carbon footprint, a decision has been made to close both major coal-fueled power plants at Hadera and Ashkelon in the future, and to convert them to gas fueled units. Apart from renewable energy, this will render NG as the sole source of energy for electricity in the country. The Ministry of Energy plan is aimed at fulfilling Israel's role in the agreement and at promoting an efficient, green economy. The objective is to generate up to 30% of electricity using renewable energy by 2030, and potentially generate up to 100% of electricity this way by 2050. The increasing share of renewable energy presents several challenges in the interim however, particularly with regard to the effects on the natural gas system, which must balance the intermittent and variable electricity production of uncontrollable renewable sources.

As of 2020, more than 50% of Israel's electricity is produced from NG. The yearly demand for NG recently increased beyond 11 billion cubic meters (BCM). During the transition to the 2030 goal, that share is expected to increase up to 80%-85% in certain years. Moreover, two agreements were signed

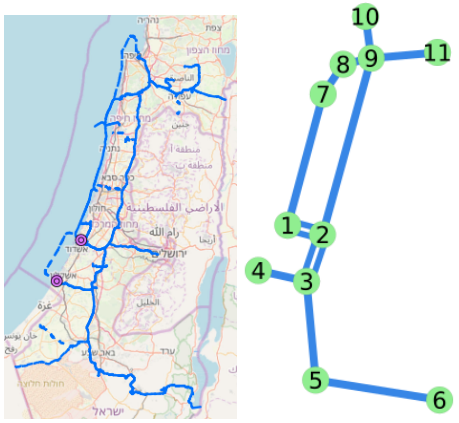

#	n_s	n_e	L	D
1	1	2	26	600
2	2	3	28.5	600
3	3	4	25	600
4	3	5	56	600
5	5	6	81	445
6	1	7	77	736
7	7	8	22	757
8	8	9	14	743
9	2	9	102	914
10	9	10	34.4	766
11	9	11	34.4	914
12	1	2	26	914
13	2	3	28.5	914

Figure 4: Description of the Israeli gas system: (left) Sketch of the true system. (center) Map of the reduced 11-node system that we use for this study. (right) List of pipelines in the simplified system. Their start node (n_s), end node (n_e), length L in km, and diameter D in mm.

with Egypt and Jordan stipulating that Israel will export 130 BCM of NG from the Leviathan and Tamar gas fields over the next ten years. (At the moment, the non-electricity end use of NG in Israel is small, amounting to around 9000 MMBTU/h or around 10% of the hourly typical flow). Those data show that there are many issues surrounding the NG network in Israel over the next decade.

https://www.noga-iso.co.il/en/NOGA, Israel Independent System Operator (IISO), is the newly founded Israeli Electric System Operator. Its mandate is to act to ensure continuous electricity supply, at the required reliability and quality level, to all electricity consumers, in normal and emergency system conditions, and to manage the wholesale electricity market operations competitively and equitably. In addition to managing day-to-date operations, IISO is also in charge for planning development of the generation system, including recommendations for the required generation and storage capacity, maintaining optimal mix, location and timing for integration of generation and storage facilities. IISO is tasked to set up criteria for planning the development of the generation system. The company mandate also includes many other aspects of the transmission system planning, such as related to data forecast, transformer placement and characterization and, overall, formulation of a multi-year plan for the transmission system development. It is recognized, that to achieve all the goals IISO needs state-of-the-art tools to model the Natural Gas system and its interaction with the Electricity network.

Jean, this is placeholder for you to describe how the small Israel gas model was designed (main principles, consideration, data) ... we may then extend https://www.overleaf.com/project/62bca to building medium/large models and also to building respective power system models of Israel with a clear cross-links between the two infrastructures (see also discussion below) ... We have built a model for Israeli gas system based purely on public data available on the Internet. The data source is the website of the Israel Natural Gas Authority www.ingl.co.il. We have in fact built two models:

1. A simple toy-model which comprises 11 nodes and 12

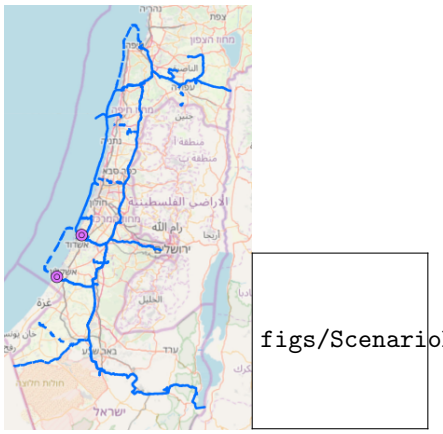

Figure 5: Comparison of the actual and reduced models of the NG network of Israel.

#	Height (m)
1	1
2	65
3	140
4	0
5	361
6	-371
7	-55
8	0
9	130
10	0
11	175

#	Start	End	Length (km)	Diameter (mm)
1	1	2	26	600
2	2	3	28.5	600
3	3	4	25	600
4	3	5	56	600
5	5	6	81	445
6	1	7	77	736
7	7	8	22	757
8	8	9	14	743
9	2	9	102	914
10	9	10	34.4	766
11	9	11	34.4	914
12	1	2	26	914
13	2	3	28.5	914

Table 1: Characteristics of the pipes in the reduced NG model of Israel gas built based on the publicly available data. Left table: list of nodes. Right table: list of pipes.

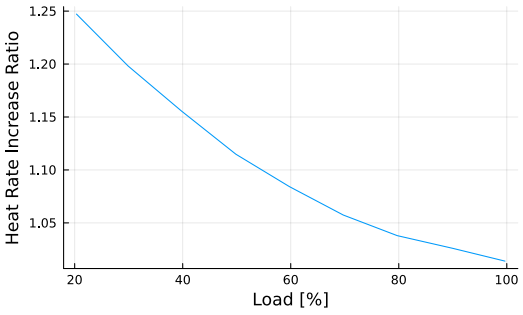

Figure 6: Typical Gas Turbine Efficiency Curve

pipes; we will present this model thoroughly in this report

2. A more detailed model (XX nodes and YY pipes) which will be discussed in the next report

In this manuscript we present a reduced, schematic gas model of Israel based on open-source public resources, shown in Figure 4. The data source is the website of the Israel Natural Gas Authority www.ingl.co.il. In order to perform the simulations, we need to create time series of the gas withdrawals at the model nodes. To do this, we use public data published by the Electricity Authority from the website https://www.gov.il/he/departm The data are in the form of half-hourly time series of electricity production (in MW) at all units. We convert the power data to gas consumption with the help of typical gas turbines efficiency curves (see Figure 6 for an example of such a curve).

6 Dynamic Modeling of Pipe Flow

We utilize dynamic modeling discussed in [**?**, **?**, **?**] (see also references therein) and specific algorithmic scheme from [**?**] called https://github.com/kaarthiksundar/GasTranSim.jlGasTranSim implemented by Los Alamos National Laboratory team in Julia [**?**].

Basic equations, expressing conservation of mass and momentum and describing flow of gas in a single pipe (with gas velocity much smaller than the speed of sound), are [**?**, **?**]:

$$\partial_t \rho + \partial_x \phi = 0, \tag{11}$$

$$\partial_t \phi + \partial_x p = -\frac{\lambda}{2D}\frac{\phi|\phi|}{\rho}, \tag{12}$$

where $\rho(t;x)$, $\phi(t;x)$ and $p(t;x)$ are the gas density, mass flux and pressure measured at the moment of time t at the position x along the pipe; λ is the Darcy-Weisbach friction factor of the pipe (per diameter, D). Eqs. (11) -(12) are supplemented by the equation of state, relating pressure and density

$$p = Z(\rho, T)RT\rho \tag{13}$$

In this study we use the CGNA formula for $Z(\rho, T)$, see e.g. [**?**].

$$p = ZRT\rho, \tag{14}$$

where the compressibility factor, Z, dependent on temperature is a function of temperature computed according to the standard CGNA formula [**?**]. Effects of gravity and temperature variations along the system are ignored, as the effects are small and our representation is schematic [1].

[1] Taking into account the temperature variations is only important in countries with sub-zero winter temperatures. In Israel, this is not the case and we make the assumption of a constant temperature equal to 15 Celsius degrees. Accounting for the effects of elevation/gravity is of a concern only at the node #6, located in the Dead Sea area, roughly 400 meters below the sea level, and at the node # 5, located close to Beer-Sheva at 300 meters above the sea level. Given that ignorning this effect results only in a relatively minor pressure drop of 3 to 5 bars in the southern part of the system, we ignore it for now in the simplest version of the model.

The single pipe description extends to a system of pipes. Each pipe is characterized by three parameters: diameter, length, and the friction factor per diameter. Each node prescribes a boundary condition for one side of (at-least) one pipe at all instances in time. Additionally, nodes and pipes are joined via condition of mass conservation (Kirchoff's rule, that the mass entering a junction must equal the mass exiting the junction). As is standard, demand nodes specify a flux withdrawal as a function of time. The system in question however, additionally specifies flux at supply nodes. Thus all supplied boundary conditions are on flux.

Denoting ρ_{ij}, ϕ_{ij} to be the dynamic variables on the pipe from node i to node j, and ρ_n, ϕ_n to be the density and flux at node n, we write the full system to be solved as:

$$\partial_t \rho_{ij} + \partial_x \phi_{ij} = 0 \tag{15}$$

$$\partial_t \phi_{ij} + \partial_x p_{ij} = -\frac{\lambda_{ij}}{2D} \frac{\phi_{ij}|\phi_{ij}|}{\rho_{ij}} \tag{16}$$

subject to initial and boundary conditions:

$$\rho_{ij}(x,0) = \rho_{0,ij}(x) \tag{17}$$

$$\phi_{ij}(x,0) = \phi_{0,ij}(x) \tag{18}$$

$$\phi_n(t) = d_n(t) \tag{19}$$

$$\sum_{j \in \mathcal{E}} \phi_j S_{ij} + d_j = 0 \tag{20}$$

Where S_{ij} is the cross-section of the pipe. Initial conditions for density and mass-flux in the system are constructed based on actual operational data. To solve for dynamics of mass flows and pressures across the system we use the staggered-grid approach of [**?**] which is an explicit, conservative, second order, finite difference scheme, stable given a CFL condition is satisfied. We remind that, as of now, the Israel system does not contain compressors. This approach solves the governing system of PDEs, **??**,**??** on two separate grids.

Then, on these grids we can write $\rho(\tau_n, \xi_j) = \rho_n^j$. Using finite difference, and defining $\beta = \frac{\lambda L}{2D}$, we write the dynamical equations **??**, **??** in the discretized forms:

$$\frac{\rho_j^{n+1} - \rho_j^n}{\Delta\tau} + \frac{\phi_j^m - \phi_{j-1}^m}{\Delta\xi} = 0 \tag{21}$$

$$\frac{\phi_j^{m+1} - \phi_j^m}{\Delta\tau} + \frac{\rho_{i+1}^{n+1} - \rho_i^{n+1}}{\Delta\xi} = -\beta \frac{(\phi|\phi|)_j^{n+1}}{\rho_j^{n+1}} \approx -\beta \frac{(\phi|\phi|)_j^{m+1} + (\phi|\phi|)_j^m}{\rho_{i+1}^{n+1} + \rho_i^{n+1}} \tag{22}$$

$$\implies \phi_j^{m+1} + \beta\Delta\tau \frac{(\phi|\phi|)_j^{m+1}}{\rho_i^{n+1} + \rho_{i+1}^{n+1}} = \phi_j^m - \frac{\Delta\tau}{\Delta\xi}\left(\rho_{i+1}^{n+1} - \rho_i^{n+1}\right) - \beta\Delta t \frac{(\phi|\phi|)_j^m}{\rho_i^{n+1} + \rho_{i+1}^{n+1}} \tag{23}$$

We can solve the former to find an equation to advance ρ:

$$\rho_j^{n+1} = \left(\frac{\phi_{j-1}^m - \phi_j^m}{\Delta\xi}\right)\Delta\tau + \rho_j^n \tag{24}$$

However, the discretized momentum equation 22 is implicit.

Labeling y as the RHS of 22, i.e.,

$$y = \phi_j^m - \frac{\Delta\tau}{\Delta\xi}(\rho_{i+1}^{n+1} - \rho_i^{n+1}) - \beta\Delta\tau \frac{(\phi|\phi|)_j^m}{\rho_i^{n+1} + \rho_{i+1}^{n+1}} \tag{25}$$

We have an equation of the form:

$$F(x) = y \tag{26}$$

$$x = \phi_j^{m+1} \tag{27}$$

$$F(x) = x + \beta\Delta\tau \frac{(x|x|)}{\rho_i^{n+1} + \rho_{i+1}^{n+1}} \tag{28}$$

We can write the inverse of F as

$$x = F^{-1}(y) = \text{sign}(y)\frac{-1 + \sqrt{1 + 4a|y|}}{2a} \tag{29}$$

And because we know the value of y, we can readily solve for $x := \phi_j^{m+1}$.

7 Operational Scenarios

We search for robustness in the face of challenging scenarios. To this end we construct scenarios that represent two basic phenomena:

- Moderate uncertainty at demand nodes, represented through addition of a random noise at the consumption site, e.g. associated with response of gas-generators to renewable fluctuations on the electric-side of the system.

  $$d_i(t) \to X_i(t) \tag{30}$$

  where

  $$dX_i(t) = \alpha(d_i(t) - X_i(t)) + \gamma dW \tag{31}$$

  is a Ornstein–Uhlenbeck process - designed so that the mean is our nominal demand, $E[X_i(t)] = d_i(t)$, and the variance approaches a constant exponentially fast:

  $$\text{Var}(X_i(t)) = \frac{\gamma}{2\alpha}\left(1 - e^{2\alpha t}\right) \tag{32}$$

  The parameters were tuned heuristically to ensure α the mean was respected, and the variance approaches

  $$\text{Var}(X_i(t)) \approx 0.01\mu_i^2 \tag{33}$$

  With μ_i being the mean withdrawal of node i. The noise for each demand is uncorrelated, a conservative approach which ignores geography and climate scales. Implementation on an actual system should be accompanied with data analysis and forecasts to determine realistic noise types for demands.
- Abrupt changes – which we coin *insults* – that occur due to malfunction, weather or other exogenous circumstance. We focus particularly on supply challenges. That is, given a supply profile $s(t)$

  $$s(t) \to s(t) + \Theta(t - T)\Gamma(t) \tag{34}$$

  where Θ is the Heaviside function, T is the time of insult, and Γ is the perturbation. For example, $\Gamma(t) = -s(t)$, simulates a complete loss of supply at time T.

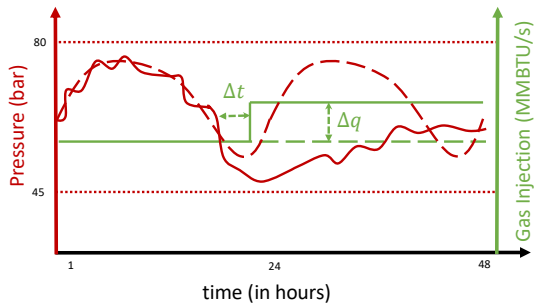

Figure 7: Schematic illustration of the use cases of the system operations during an exemplary period of 48 hours. We show forecasts (long-dashed curves) and actual profiles (solid curves) for a pressure at a node and an injection at an entry point to the system, where a control is applied in response to an insult. See text for details.

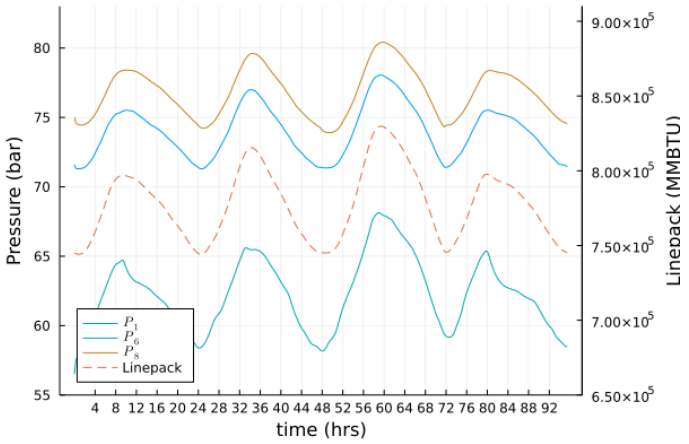

Figure 8: Nominal week in August, with no uncertainty.

In addition to studying bare "do nothing" scenarios we will also analyze mitigation by controls. We assume that controls at the injection points (off-shore extraction sites at node #1 and node #8 in Fig. 4) and consumption sites, are step-wise. Operationally - due to the close coupling of Israel's gas extraction and delivery - step-wise control is preferable on the supply-side, while significantly idealized for demand nodes.

Focusing on the most challenging cases on fast ramps up (and, possibly, ramps down too) of consumption, e.g. around the time of sundown (or sunrise) in winter, we limit our analysis in this manuscript to *prescribed* control. This allows us to conduct intuitive and easy to interpret tests of possible options. The goal of this exploration is to analyze how the system operator can manage gas transients in line pack, meet power demand evolving throughout a day (or a number of days) while also not exceeding the gas system pressure constraints.

Our approach is illustrated schematically in Fig. (7). Long-dashed green curve shows injection profile on one of the entry points to the system. Typically, it is flat where the value (in $MMBTU/s$) is computed based on the balanced forecast of consumption over the entire system and on the operational split of responsibilities between the injection points. Long-dashed red curve illustrates forecast for a pressure at a node of the system. Solid red curve shows an actual pressure profile, which, subject to typical uncertainty, largely follows the forecast till $\approx$ (hour) 23:00, when a significant insult occur and the deviation from the forecast becomes significant. Short-dashed red curves mark node-specific upper and lower limits for the pressure profile. Solid green curve shows operation profile at the injection point, which remains operational (in this use case) through out the 48 hours of observation, however the actual injection profile is not flat – it follows forecast till hour $\approx$ 23:00+Δt when a step-wise control action, responding to the $\approx$ 23:00 emergency, is applied. Selection of the proper time delay Δt, of the control response, and of the respective amplitude, Δq, constitutes a major operational challenge.

The approach to monitoring and prescribed control of the system is summarized in Table **??**. We present six scenarios of progressive stress. Each scenario is illustrated with a figure summarizing respective dynamics. (Animations of the pressure timeseries across the network, as well as software and data to reproduce all the results included here, can be found at https://github.com/cmhyett/FluxControlLinepack.)

We define a pressure crossing as when the nodal pressure falls below 50bar. The survival time τ is defined as the time between initiation of the insult and the time to first pressure crossing *at any node*. Note that due to integrated random fluctuations of demand, we obtain distributions of survival times, shown for example in figure[12] as a shaded region about the median, annotated above with the node at which the pressure crossing occurred. To keep the picture clear, the figures only show pressure crossings for a subset of our nodes, namely 9,1, and 6, as they yield information regarding the north, middle and south of our network respectively.

1. Fig. (8) shows pressures (dashed) and linepack (solid), in a flux-controlled, nominal week in August. It serves as our base case, and importantly, because of the constant flux at supply nodes, the temporal variation of pressure across the network is governed by the intra-day demand fluctuations.

2. Fig. (9) adds random fluctuations to demands on this nominal week - modeling uncertainty from exact power demand and generation of renewables. For each node, we add noise distributed uniformly with width of 5% of nominal demand at that node. These small perturbations integrate over time, leading to significant linepack and pressure deviations from the mean.

3. Fig. (10) introduces an "insult" indicating off-nominal or emergency operation. Particularly, supply at node #1 (one of our two supply nodes) are closed at hour 36 in the simulation. We continue to run the simulation to observe the rate of linepack decay and the sequence of pressure crossings. The survival time in this scenario is

$$\tau = 4.13 \pm 0.38 \text{ hrs} \tag{35}$$

   where the 0.38 is the standard deviation. This information can be translated to spatiotemporal "vulnerability" of the gas network.

4. Fig. (11) introduces the same insult as scenario 3, but at hour 48 instead of hour 36. In particular, this corre-

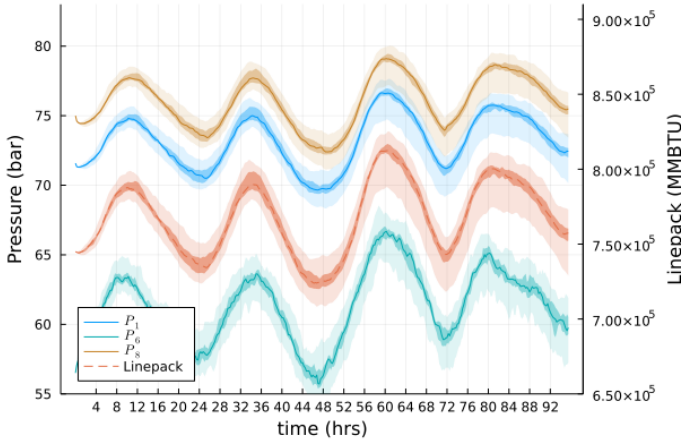

Figure 9: Nominal week in August, with empirical noise added to demand curves. Notice the drift of linepack and pressure jitter, consistent with what was predicted in [**?**]. Using a Monte-Carlo with 50 simulations, we plot filled regions of containing the middle 75%, 25%, and median using increasing color intensities.

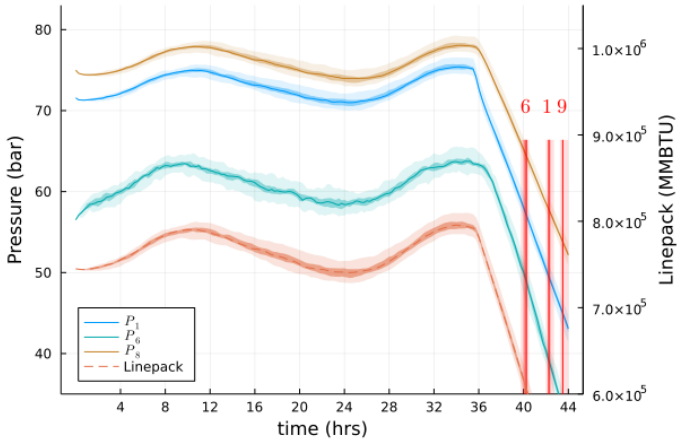

Figure 10: Scenario 3 results, an insult at a crest of the linepack at $t = 36$hrs. Using a Monte-Carlo with 50 simulations, we plot filled regions containing the middle 75%, 25%, and median using increasing color intensities.

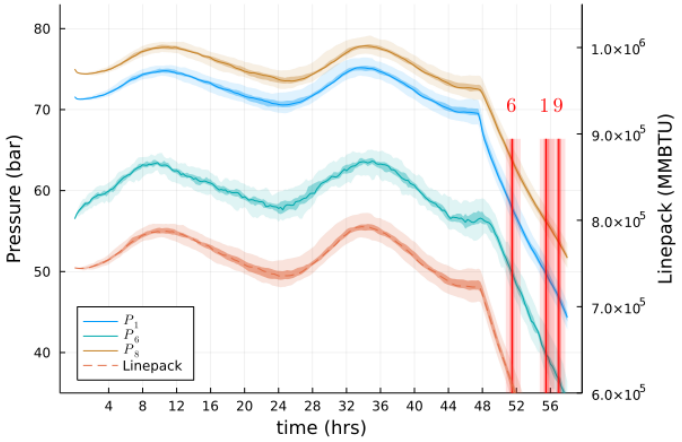

Figure 11: Scenario 4 results, an insult at a trough of the linepack at $t = 48$hrs. Using a Monte-Carlo with 50 simulations, we plot filled regions containing the middle 75%, 25%, and median using increasing color intensities.

sponds to the insult occurring at a trough of the linepack curve instead of a peak. We highlight first that the time to first pressure crossing survival time is shorter in this case

$$\tau = 3.58 \pm 0.89 \text{ hrs} \tag{36}$$

This simple statement that the survival time of the network depends on the start time of an insult is the result of complicated interactions between demand-node boundary conditions as well as network topology.

5. Fig. (12) begins introducing control, attempting to mimic "human in the loop" control of the network under the insult described in scenario 4. In this scenario, the operator at the remaining supply (node 8), increases to the max flow-rate a half hour after the insult begins ($t = 48.5$hrs). This control stabilizes the linepack in the short-term, but fails to handle the daily ramp near hour 60. In particular, the south of the network, far from the remaining supply contains all of the pressure crossings.

$$\tau = 14.17 \pm 4.07 \text{ hrs} \tag{37}$$

6. Fig. (13) finally builds upon scenario 5 to additionally curtail demand 2 hours after the insult ($t = 50$hrs). This translates to a variety of potential action, from high penalty demand-response (as demonstrated during heat waves in California) to the transition of natural gas plants to alternative fuels, or the utilization of stored power.

7.1 Illustrative Example

For example, in the case of the prescribed control at a supply node of the Israel gas system, modeled by Eqs. (11,12) extended to multiple pipes and accounting for injections/consumption at the nodes and for the fields continuity across the network, we pose the following question: if we can only control the supply via discrete jumps when should we introduce a perturbation (and of what magnitude) at the supply nodes to

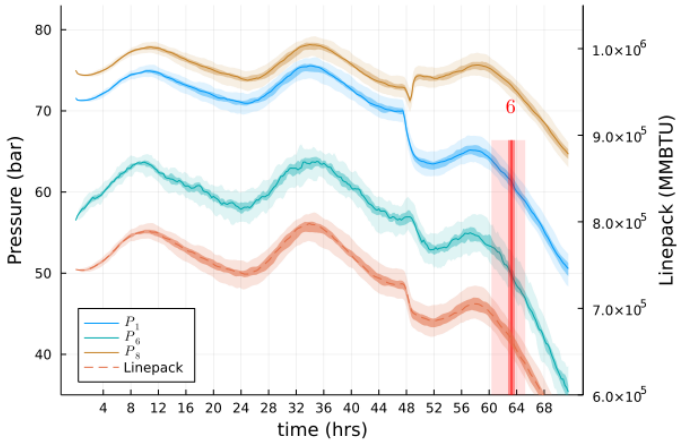

Figure 12: Scenario 5 results, introduces a step-wise increase in supply at node 8 half an hour after the insult ($t = 48.5$hrs).

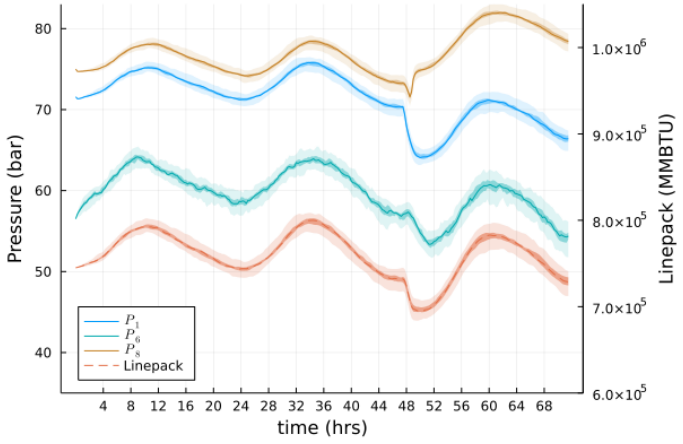

Figure 13: Scenario 6 results, curtails demand at $t = 50$hrs, to maintain minimum pressures across the network.

meet evolving (and also fluctuating demand), while keeping pressure relatively flat? In other words, we want to increase supply to match additional demand, with the objective to minimize the pressure deviations somewhere, e.g. at the supply, at the demand or, perhaps, somewhere in the middle.

Criston, I suggest the following modification of the two schematic figures, Fig. (14) and Fig. (7.1).

In the improved version of Fig. (14) I suggest to show:

- Pressure at a node of the network (left) vs adjustment of the injection/withdrawal at a control node. (Showing the case of flow control will make it a bit more clear — will help to avoid confusion about two different pressures we need to discuss in the case when we have a pressure control. Having said this, we may want to mention after the illustrative example is shown that the pressure control is another option we will also consider in the manuscript.)

- For the pressure profile – show (a) an evolving pressure forecast curve for the node, (b) an actual curve with a clear departure from the forecast, presumably associated with an insult, (c) corrected curve dependent on the timing and amplitude of the injection/withdrawal correction (may be good to show 2-3 options), (d) straight lines associated with upper and lower limits allowed at the node.

- For the profile of injection/withdrawal at a node – show (a) forecast curve for the control node injection/withdrawal, (b) the (2-3) corrected option(s) equivalent to what we show for the pressure.

Wrt Fig. (7.1). I am not sure we want to discuss the 5-node example in the paper. However, if we do, the 5 node example needs to be defined in words or shown in a figure.

The schematics of the prescribed control is shown in Fig. (14). Given a perturbation, e.g. perturbation of the withdrawal at the seconds of the abrupt (insult) type, we adjust (increase) supply changing it in a step-wise manner and probing different timing and amplitude of adjustment. Add brief description, clear and preferably without formulas. To illustrate, consider a 5-node example shown in Fig. ?? Criston, please add figure showing the 5-node example.

denote step-wise control at a single supply node, s , $c(t;x)$ at a single supply node s, and introduce our perturbation there. Further, let the boundary condition at s be on pressure, and suppose that it is constant $p_s(t) = P$. Then, the control becomes, $c(t;x) = c_s(t) = dP \cdot \Theta(t - t_0)$, where $\Theta(x)$ is the Heaviside function and the boundary condition is

$$p_s(t) = \begin{cases} P & \text{if } t < t_0 \\ P + dP & \text{if } t \geq t_0. \end{cases}$$

Suppose now that the location in which we want to minimize variation is x_0. Changing $c(t;x)$ we seek to minimize the maximal value (over the network) between the perturbed and nominal values of the pressure. A simple approach to addressing this optimization question consists in looking for the point when the additional supply be felt at a demand node. In other words, we are asking what is the time delay

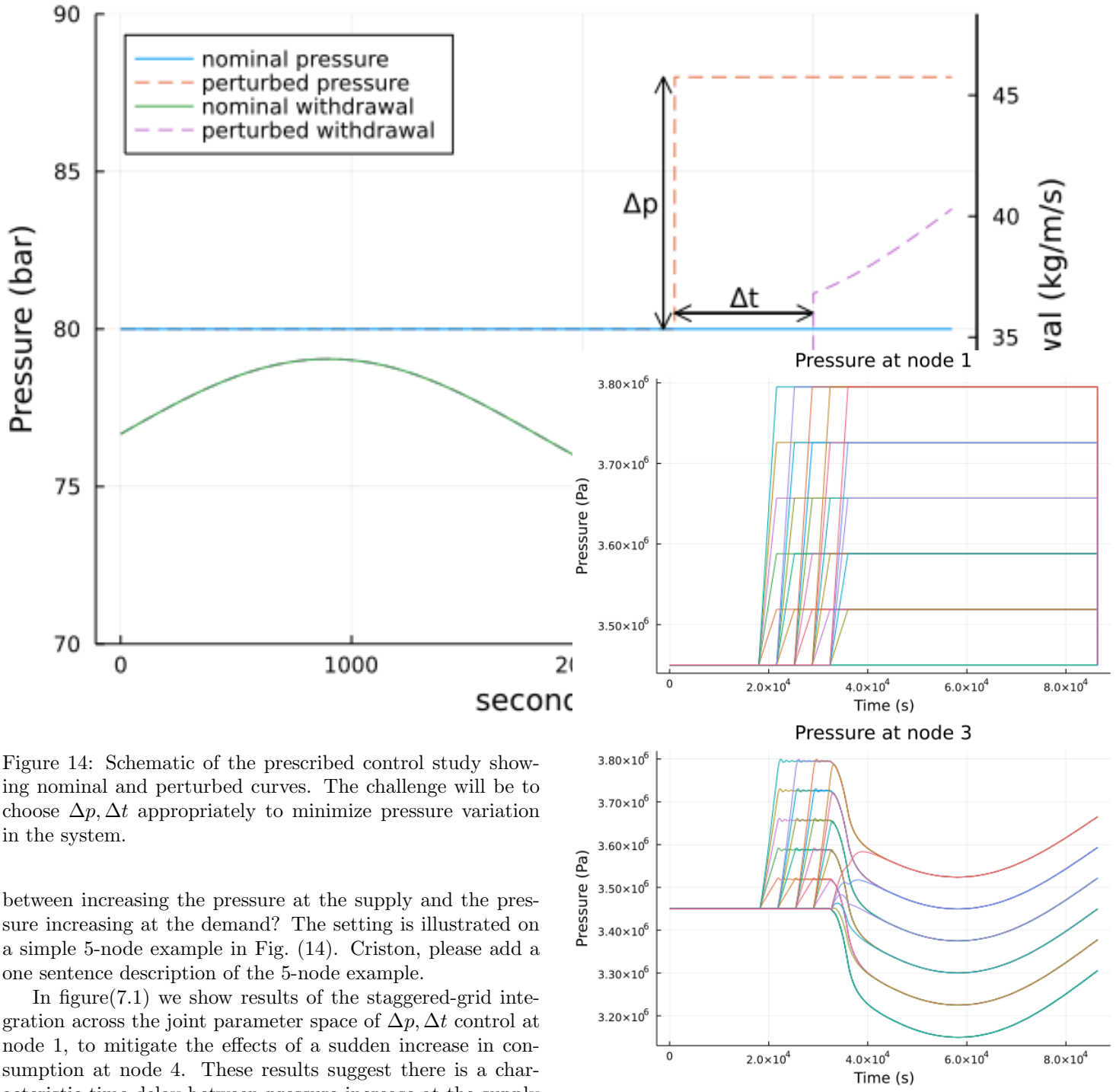

Figure 14: Schematic of the prescribed control study showing nominal and perturbed curves. The challenge will be to choose $\Delta p, \Delta t$ appropriately to minimize pressure variation in the system.

between increasing the pressure at the supply and the pressure increasing at the demand? The setting is illustrated on a simple 5-node example in Fig. (14). Criston, please add a one sentence description of the 5-node example.

In figure(7.1) we show results of the staggered-grid integration across the joint parameter space of $\Delta p, \Delta t$ control at node 1, to mitigate the effects of a sudden increase in consumption at node 4. These results suggest there is a characteristic time-delay between pressure increase at the supply node 1, and the consumption node. This timescale can be found by computing the minimal path length ℓ, and dividing by the characteristic velocity $u_0 = \phi_0/\rho_0$, $\tau = \ell/u_0$.

In figure (1) bar is used for pressure, in figure (2) Pa is used, I think they should use same units.

8 Monotonicity

In our scenario selection, we were intentionally coarse, preferring severe and abrupt challenges, while searching for the mildest controls for remedies. This is intentional, as previous work has given us monotonicity guarantees [**?**, **?**]. That is, we have that for any less-severe challenge (as in the more physically realistic scenario of a slow ramp down of a supply instead

of our simulated near-immedate shut off), our pressures will be bounded below by the most severe case, and thus in turn our estimates for survival times are in fact lower, conservative bounds.

We advocate this approach for schematic expositions as it is only with full operational and procedural knowledge that one can obtain tight estimates - that is, work inherently reliant on proprietary data.

It should also be noted that monotonicity can yield bounds for the more usual scenario of pressure and linepack drift resulting from integration of stochasticity due to renewables, such drift can be seen in Fig.9. However, monotonicity bounds were derived without relation to probability, thus it is likely that future work can tighten these bounds, avoiding expensive simulation except when full distributional knowledge is needed.

I suggest to also add here discussion of monotonicity. Specifically, we would like to state what it means, with reference to [**?**, **?**], and then explain that it allows to generalize results of the use-cases just discussed significantly. Explain (on examples) that the monotonicity guarantees, in particular, that the reserve time estimated for a "larger insult" is shorter than the reserve time of a "smaller" insult. Criston, please extend this part. Do we need an extra figure to illustrate it?

9 Conclusion

We investigate the spatiotemporal response of a reduced model of Israel's NG network to prescribed insults and human-in-the-loop controls in order to evaluate robustness and suggest control strategies. To reiterate, Israel's network is unique because of the absence of a compressor, and that the inlets specify flux, not pressure. Further, we perform this study looking towards the increased importance of NG to mitigate increasing stochasticity in demands expected in the coming years as coal is phased out, and renewables grow.

The specification of flux vs pressure leads to the pressure timeseries of the network being dominated by daily demand curves as shown in Fig. (8), increasingly susceptible to pressure drift from stochastic fluctuations in nominal demands.

Further, we call out the importance of robustness of the network not simply to insults, but to insults at any time - leading to the idea of "system reserve" being time and spatially dependent.

Future work will improve on modeling to more completely capture uncertainty propagation through the network, and its influence and interaction with control strategies. We envision extending the prescribed control, also reinforced by monotonicity [**?**, **?**], developed in this manuscript with the powerful optimization approaches developed to account for dynamic optimization over compressors [**?**, **?**, **?**, **?**, **?**], e.g. to evaluate benefits of adding compressors to the NG system of Israel. We also plan to carry on a comprehensive modeling and control of the combined power and gas system of Israel, in the spirit of the approach highlighted in [**?**, **?**].

10 Differentiable Simulators for Gas-Aware Unit Commitment

Differentiable Programming is a paradigm in which automatic differentiation is applied to general computer programs. It began after the popularity of structured or physics-informed neural networks led to increasing interest in using dynamical systems theory in machine learning e.g., ([**?**]).

Differentiable Simulation (DS) is a particular case, where the program of interest is a dynamical systems model. It can be thought as one implementation of PIML, wherein the data (usually spatiotemporal) is thought to be described by a partially known ODE. In applications where the underlying physics is partially known, DS can be *very* efficient, and like other applications of PIML, can improve generality by removing out-of-distribution sampling issues present in black-box NNs. Further, learning is likely more rigorous, as the known-portion of physics is as well approximated as in a direct simulation.

Our example of DS is in enriching unit commitment with knowledge of transient states of the gas system model. To do this, we need to illucidate both aspects.

10.1 Gas Dynamics

10.2 Optimal Power Flow

11 Dynamical Systems

12 Machine Learning

13 Conclusion & Prospectus